THE JOURNAL OF PHYSICAL CHEMISTRY C

Article

pubs.acs.org/JPCC

Synthesis, Structural, Magnetic, and Electronic Properties of Cubic $CsMnMoO_3F_3$ Oxyfluoride

Victor V. Atuchin,*[,†] Maxim S. Molokeev,[‡] Gleb Yu. Yurkin,[‡] Tatyana A. Gavrilova,[†] Valery G. Kesler,[†] Natalia M. Laptash,[§] Igor N. Flerov,[‡,∥] and Gennadii S. Patrin[‡,∥]

[†]Institute of Semiconductor Physics, SB RAS, Novosibirsk 630090, Russia

[‡]Institute of Physics, SB RAS, Krasnoyarsk 660036, Russia

[§]Institute of Chemistry, FEB RAS, Vladivostok 690022, Russia

[∥]Institute of Engineering Physics and Radio Electronics, Siberian Federal University, Krasnoyarsk 660074, Russia

Supporting Information

ABSTRACT: A powder sample of $CsMnMoO_3F_3$ oxyfluoride has been prepared by solid state synthesis. The pyrochlore-related crystal structure of $CsMnMoO_3F_3$ has been refined by the Rietveld method at T = 298 K (space group Fd-3m, a = 10.59141(4) Å, V = 1188.123(8) Å^3; R_B = 3.44%). The stability of the cubic phase has been obtained over the temperature range T = 110−293 K by heat capacity measurements. Magnetic properties have been measured over the range of T = 2−300 K. The electronic structure of $CsMnMoO_3F_3$ has been evaluated by X-ray photoelectron spectroscopy. Chemical bonding effects have been discussed for all metal ions using binding energy difference parameters and wide comparison with related oxides and fluorides. The competition between O^{2-} and F^- ions for metal valence electrons has been found.

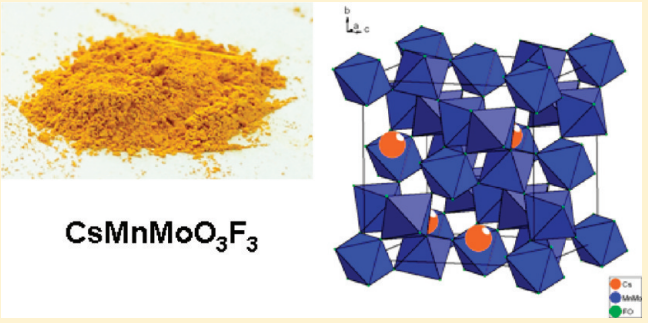

INTRODUCTION

Oxyfluorides containing the six-coordinated quasi-octahedral species $(MF_xO_{6-x})^{3-}$ with fluorine/oxygen ligands are of great interest due to intriguing structural behavior.[1−5] The compounds with the $(MO_3F_3)^{3-}$ groups in a crystal lattice, however, keep rather often a cubic structure in spite of anion pseudo-octahedral local symmetry. These units are inherently strongly polar due to the displacement of a central atom toward oxygen atoms. There exist at least two reasons for canceling the separate octahedron dipole moments associated with the F/O ligands disordering and/or with the relative orientations of neighboring octahedral units. Such a situation is realized, for instance, in two crystal families with the following general formulas: $A^+_2(A^+)'MO_3F_3$ and $A^+A^{2+}MO_3F_3$ (M = hexavalent transition metal). They are characterized by an elpasolite-type crystal lattice (space group Fm-3m, Z = 4)[6] and defect pyrochlore structure (space group Fd-3m, Z = 8) related to $RbNiCrF_6$, respectively.[7,8]

Rather intensive investigations of elpasolite-like oxyfluorides $A^+_2(A^+)'MeO_3F_3$ (A^+, $(A^+)'$ = Na, K, NH_4, Rb, Cs; M: Mo, W) revealed that many of them undergo, on cooling, the structural transformations associated with partial or complete ordering of fluorine/oxygen ligands disordered in the Fm-3m phase. As a result, the crystals of this family show such interesting physical properties as ferroelectricity, ferroelasticity, and great barocaloric efficiency.[9−12] Moreover, it was found that several compounds can be considered as classical multiferroics[13,14] because of the dual nature of the phase transition from a cubic phase followed by the simultaneous appearance of crystal spontaneous polarization and ferroelastic twinning. Molybdenum and tungsten compounds undergoing order−disorder transformations with a rather large and close entropy change are characterized by a strong difference in the susceptibility to hydrostatic pressure. Due to significant values of baric coefficient dT/dp, some of the former oxyfluorides show significant intensive and extensive barocaloric effects which are comparable to the electro- and magnetocaloric effects in the materials considered as prominent solid refrigerants.[12]

So far, there is poor information only about the room-temperature characteristics of $A^+A^{2+}MO_3F_3$ compounds (A^+: Cs; A^{2+}: Ni, Zn, Mn, Co; M: Mo, W).[7,8] However, from the above standpoint, these crystals having, in accordance with cubic symmetry, a fluorine−oxygen disorder can be supposed to possess the properties close to those of elpasolite-type crystals. On the other hand, magnetic compounds containing Fe and Mn elements are of great importance because of their many potential applications.[14−16] Respectively, the search for the oxyfluorides based on $(MO_3F_3)^{3-}$ anionic groups and

Received: February 29, 2012
Revised: April 21, 2012
Published: April 24, 2012

dx.doi.org/10.1021/jp302020f | J. Phys. Chem. C 2012, 116, 10162−10170

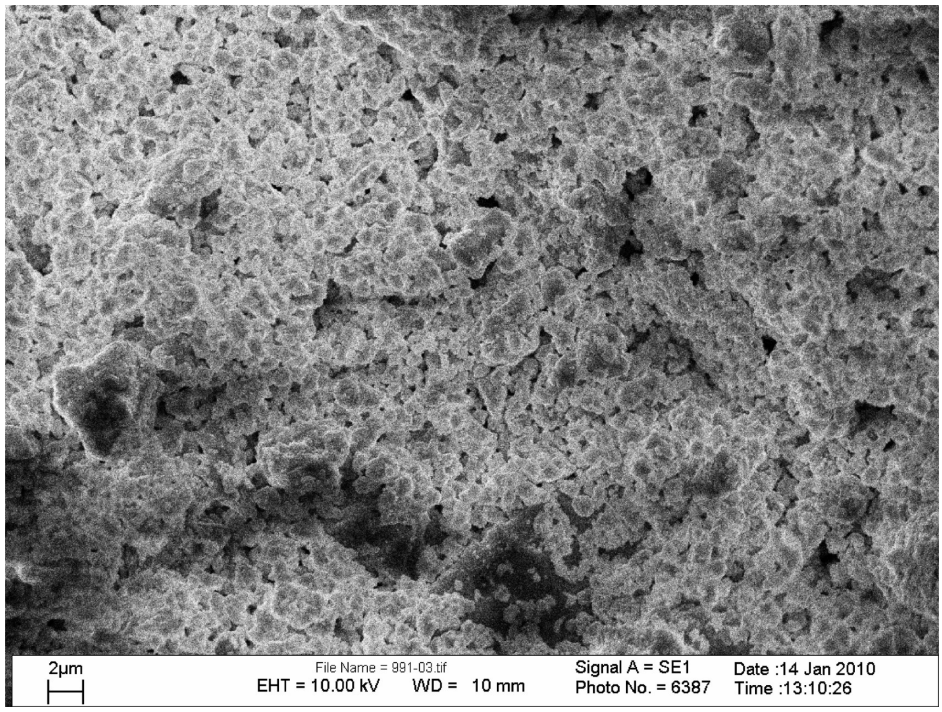

Figure 1. SEM image of $CsMnMoO_3F_3$ powder formed by solid state synthesis.

content of magnetic elements is a promising way for generation of a new class of multiferroic materials. It should be pointed out that several Mn-containing oxyfluorides with a partial substitution of F^- for O^{2-} anions were formed by fluorination in the past.[17−19] As for crystals with $(MO_3F_3)^{3-}$ groups, a compound $CsMnMoO_3F_3$, space group *Fd*-3*m*, was earlier reported but without a detailed description of structural and physical properties.[6] The present investigations are aimed at synthesizing $CsMnMoO_3F_3$ oxyfluoride and determination of the structural, thermal, magnetic, and electronic parameters over a wide temperature range.

EXPERIMENTAL SECTION

Polycrystalline $CsMnMoO_3F_3$ was synthesized in the form of yellow−orange colored powder. $(NH_4)_3MoO_3F_3$, Cs_2CO_3 (99.9%), and $MnCO_3$ (99.9%) were used as starting materials. Initially, the $(NH_4)_3MoO_3F_3$ single crystals were prepared by the method reported elsewhere.[20] The $MnCO_3$ powder was prepared by the reaction between water solutions of $MnCl_2$ (99.9%) and NH_4HCO_3 (99.9%) just before synthesis of the complex. White−pink precipitate was filtered under a vacuum and washed once with water and three times with acetone. Then the powder was air-dried under ambient conditions. The product contains 42.7 mass % of manganese that gives the overall formula $MnCO_3{\cdot}0.7H_2O$. To obtain $CsMnMoO_3F_3$, the initial components were mixed in a stoichiometric ratio governed by the reaction

$$(NH_4)_3MoO_3F_3 + 0.5Cs_2CO_3 + MnCO_3{\cdot}0.7H_2O = CsMnMoO_3F_3 + 3NH_3 + 1.5CO_2 + 2.2H_2O$$

The interaction of reagents, even at room temperature, was supported by the smell of ammonia that appeared on grinding the mixture. Solid state synthesis was produced with two stages. Initially, the powder mixture was heated in a platinum cup at T = 200−300 °C with stirring up to complete ammonia evolution. Then the powder was calcined in a closed platinum crucible at T = 500 °C for 0.5 h. The fluorine content in the final product was controlled by H_2SiF_6 distillation. The micromorphology of the final product was observed by scanning electron microscopy (SEM) with the help of an LEO 1430 device. The manganese valence state was evaluated with electron paramagnetic resonance (EPR).

The powder diffraction data of $CsMnMoO_3F_3$ for Rietveld analysis were collected at room temperature with a Bruker D8-ADVANCE powder diffractometer (Cu Kα radiation, θ-2θ geometry) and linear VANTEC detector. The step size of 2θ was 0.016°, and the counting time was 0.9 s per step. In the Rietveld refinement, we use the unit cell parameters taken from ref 1. All the refinements and data processing have been performed by the DDM program.[21] The Pearson VII function was used to model the peak profiles. The value of the sample displacement 2θ correction parameter was equal to −0.005°.

The stability of a cubic phase to the temperature change was examined by heat capacity studies over the temperature range of 110−293 K. The measurements have been performed with a differential scanning microcalorimeter DSM-10M. The powdered sample with the mass of about 0.1 g was put in an aluminum sample holder. Heating−cooling cycles were carried out in the helium atmosphere with a rate of 8 K/min. The magnetic measurements between 2 and 300 K were performed by means of a magnetic properties measurement system (MPMS, Quantum Design) on the sample with the mass of 0.0255 g.

The observation of the electronic structure of $CsMnMoO_3F_3$ was produced using the surface analysis center SSC (Riber) with X-ray photoelectron spectroscopy (XPS) method. The nonmonochromatic Al Kα radiation (1486.6 eV), with the power source of 300 W, was used for the photoemission excitation. The energy resolution of the instrument was chosen to be 0.7 eV, to have a sufficiently small broadening of natural core level lines at a reasonable signal−noise ratio. Under the

dx.doi.org/10.1021/jp302020f | J. Phys. Chem. C 2012, 116, 10162−10170

conditions, the observed full width at half-maximum (fwhm) of the Au $4f_{7/2}$ line was 1.31 eV. The binding energy (BE) scale was calibrated in the reference to Cu $3p_{3/2}$ (75.1 eV) and Cu $2p_{3/2}$ (932.7 eV) lines, assuring an accuracy of 0.1 eV in any peak energy position determination. The photoelectron energy drift, due to charging effects, was taken into account in reference to the position of the C 1s (284.6 eV) line generated by adventitious carbon present on the surface of the powder as-inserted into the vacuum chamber. Chemical composition is defined using the detailed spectra of Cs $3d_{5/2}$, Mn $2p_{3/2}$, Mo $3d_{5/2}$, O 1s, and F 1s core levels and the known element sensitivity factors.[22]

RESULTS AND DISCUSSION

The SEM image of $CsMnMoO_3F_3$ powder is shown in Figure 1. As it is seen, the sample is formed by well-coalesced agglomerates of nonfaceted particles with characteristic dimensions of ~0.5−1 μm. The high surface charging effect during SEM observation indicates a dielectric nature of the powder. Fluorine content estimated by H_2SiF_6 distillation yields the value 13.8% that is slightly lower than the value calculated for the stoichiometric composition $CsMnMoO_3F_3$ (14.7%). An observation with EPR gives a clear indication that the $CsMnMoO_3F_3$ sample under study contains manganese only in the divalent state.

Analysis of systematic extinction of the reflections proves that the space group of $CsMnMoO_3F_3$ is really *Fd*-3*m* ($Z = 8$). The main processing and refinement parameters are presented in Table 1. The coordinates of all atoms, including O and F, were defined by the Patterson method. The refinements of structure

Table 1. Main Parameters of Processing and Refinement

space group	*Fd*-3*m*
a, Å	10.59141(4)
V, Å^3	1188.123(8)
2θ-range, °	5−110
number of reflections	98
number of refined parameters	5
R_B	3.44%
R_{DDM}	8.93%
R_{wp}	17.28%

Table 2. Coordinates of Atoms, Isotropic Thermal Parameters (B_{iso}), and Occupations of Atom Positions (p) of $CsMnMoO_3F_3$

atom	*p*	*X*	*Y*	*Z*	B_{iso}, Å^2
Cs	1.0	3/8	3/8	3/8	4.82(4)
Mn	0.5	0	0	0	3.72(4)
Mo	0.5	0	0	0	3.72(4)
F	0.5	1/8	5/8	0.4308(3)	4.6(1)
O	0.5	1/8	5/8	0.4308(3)	4.6(1)

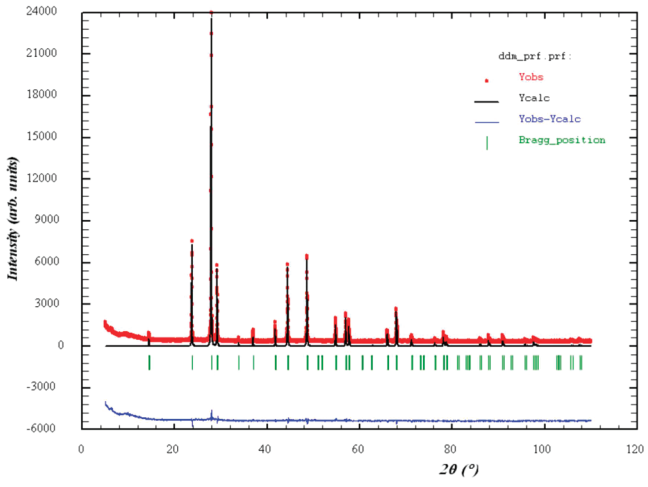

Figure 2. Experimental (red) and calculated (black) XRD patterns of $CsMnMoO_3F_3$ at room temperature.

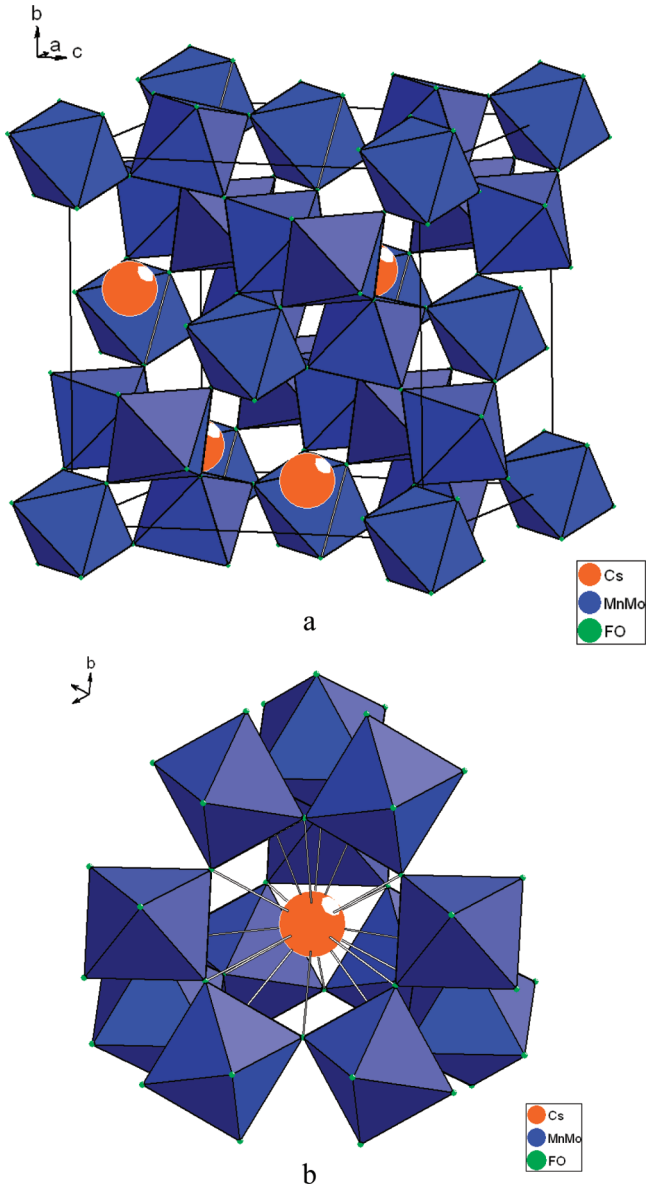

Figure 3. Crystal structure of $CsMnMoO_3F_3$ at room temperature: (a) unit cell and (b) coordination of Cs by MoO_3F_3 octahedra.

Table 3. Main Bond Lengths in $CsMnMoO_3F_3$ Structure

bond	length, Å
Mn(Mo)−F(O)	2.011(2)
Cs−F(O)	3.238(1)
Cs−F(O)[a]	3.791(2)

[a]Symmetry operation $y - 1/2$, z, $x + 1/2$.

dx.doi.org/10.1021/jp302020f | J. Phys. Chem. C 2012, 116, 10162−10170

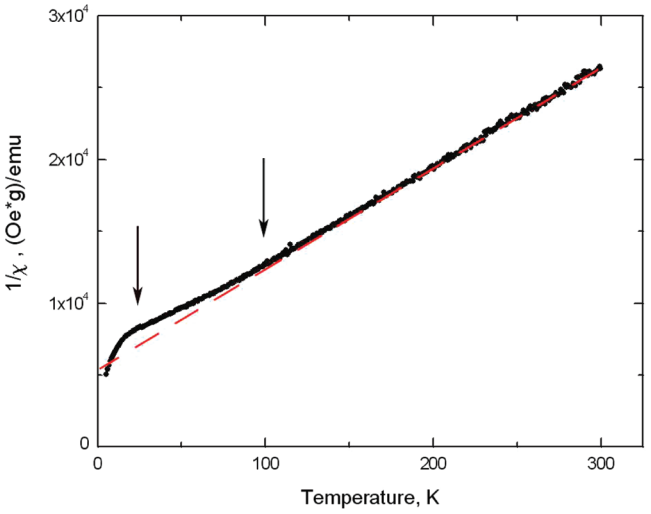

Figure 4. Temperature dependence of inverse magnetic susceptibility χ^{-1} of $CsMnMoO_3F_3$ at H = 10 Oe. Arrows indicate the temperatures of $\chi^{-1}(T)$ behavior changes.

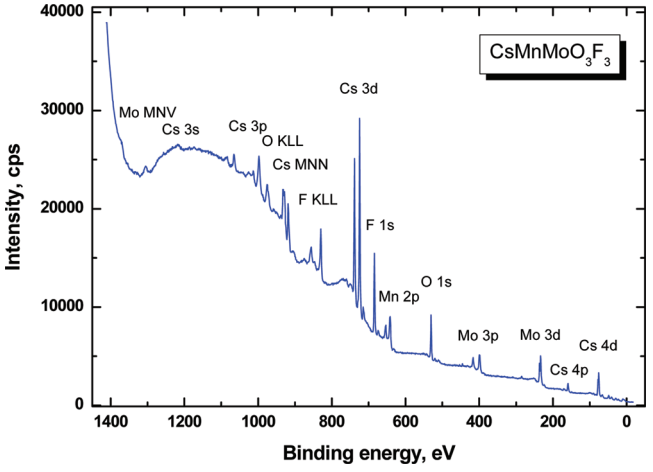

Figure 5. Survey photoelectron spectrum of $CsMnMoO_3F_3$.

lead to a drastically decreased *R*-factor and corrected model of the structure. The difference synthesis of charge density does not show any strong additional peaks. The primitive unit cell

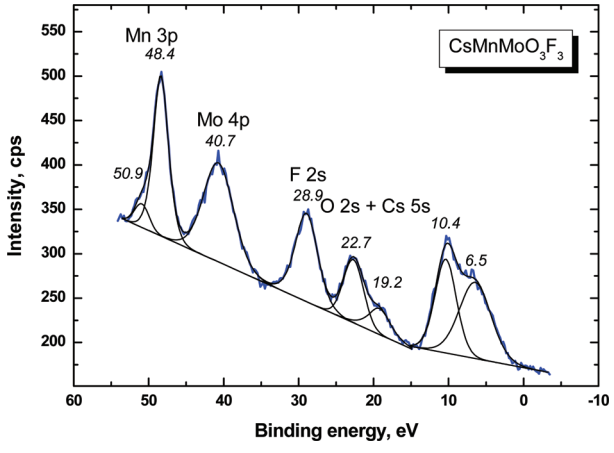

Figure 6. Valence band spectrum and upper constituent element core levels.

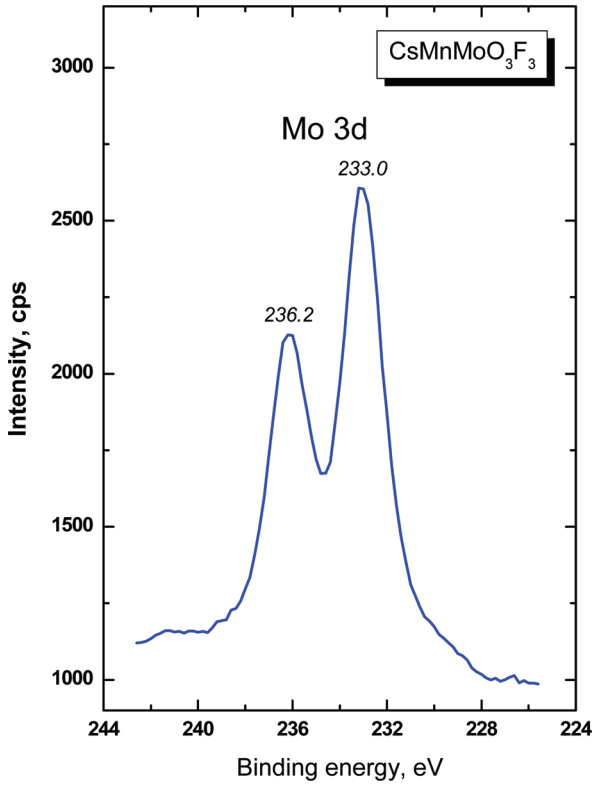

Figure 7. Mo 3d doublet in $CsMnMoO_3F_3$.

contains one Cs atom; one position in the center of the octahedron is occupied by Mn and Mo atoms in the ratio 50/50; and one position in the apex of the octahedron is occupied by O and F atoms at the ratio 50/50. Only one isotropic thermal parameter for both O/F and one thermal parameter for

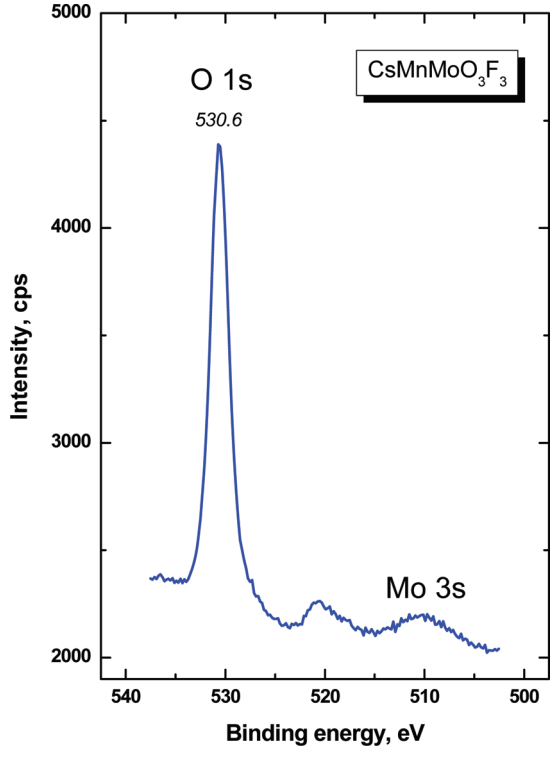

Figure 8. O 1s−Mo 3s window.

dx.doi.org/10.1021/jp302020f | J. Phys. Chem. C 2012, 116, 10162−10170

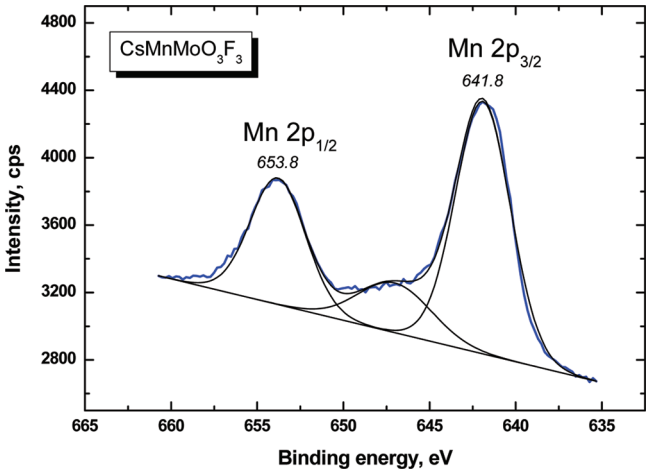

Figure 9. Mn 2p doublet recorded for $CsMnMoO_3F_3$.

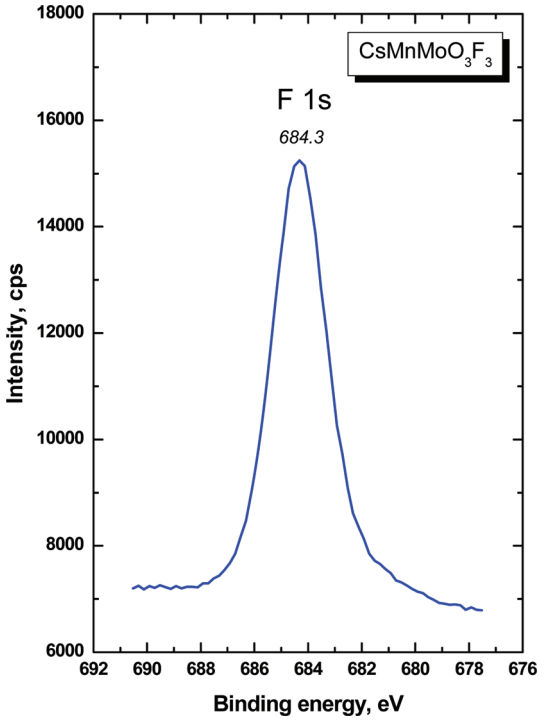

Figure 10. F 1s core level.

both Mn/Mo were refined. The value of the z coordinate of the O(F) position was refined as far as all other ions are in special positions. The coordinates of atoms, isotropic thermal parameters, and occupations are shown in Table 2. Experimental and theoretical X-ray diffraction patterns of $CsMnMoO_3F_3$ are shown in Figure 2. As shown in Figure 3, the structure has a highly developed framework of $Mn(Mo)O_3F_3$ octahedra linked to each other by common corners. Large Cs ions are in the interstices. The selected bond lengths are given in Table 3. The $Mn(Mo)O_3F_3$ polyhedron is an almost ideal octahedron. The Mn(Mo)−O(F) bond lengths are statistically equal to a value of 2.011 Å, and the angles O(F)−Mn(Mo)−O(F) are in the range of 87.3−92.6°. The Cs ion has 6 O(F) coordination with bond length d_6(Cs−O(F)) = 3.238 Å and 12 O(F) coordination with bond length d_{12}(Cs−O(F)) = 3.791 Å. So, the coordination number of Cs by O(F) is 18, and the

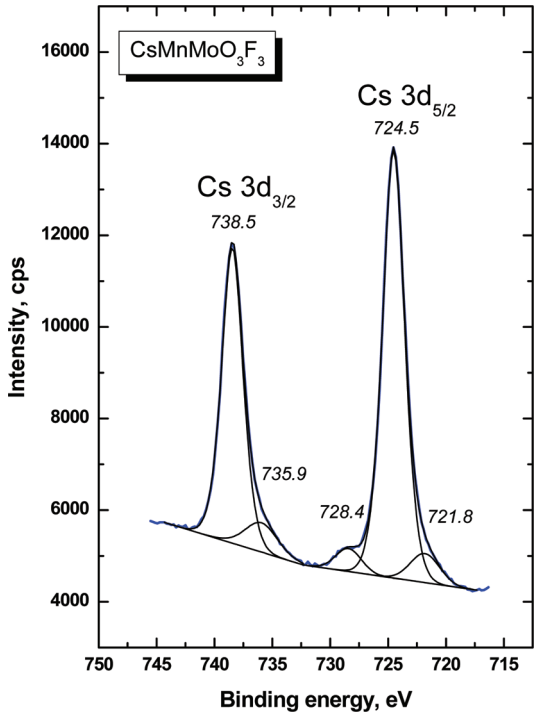

Figure 11. Cs 3d doublet recorded for $CsMnMoO_3F_3$.

Table 4. Constituent Element Core Levels and Auger Lines in $CsMnMoO_3F_3$

core level, Auger line	binding energy, eV
VB	6.5, 10.4
O 2s + Cs 5s	19.2, 22.7
F 2s	28.9
Mo 4p	40.7
Mn 3p	48.4, 50.9
Cs 4d	75.4, 77.7
Mn 3s	82.9, 89.3
Cs $4p_{3/2}$	158.9
Cs $4p_{1/2}$	170.2
Mo $3d_{5/2}$	233.0
Mo $3d_{3/2}$	236.2
C 1s	284.6, 288.2
Mo $3p_{3/2}$	399.0
Mo $3p_{1/2}$	416.5
Mo 3s	510.1
O 1s	530.6
Mn $2p_{3/2}$	641.8
Mn $2p_{1/2}$	653.8
F 1s	684.3
Cs $3d_{5/2}$	724.5
Cs $3d_{3/2}$	738.5
F $KL_{23}L_{23}$	829.7
Cs $M_4N_{45}N_{45}$	918.4
Cs $M_5N_{45}N_{45}$	928.8, 932.0
Mn $L_{23}M_{23}M_{23}$	957.4
O $KL_{23}L_{23}$	975.3
Cs $3p_{3/2}$ + O KL_1L_{23}	997.5
Cs $3p_{1/2}$	1065.1
Mo $M_{45}N_{23}V$	1305.3

coordination number of Cs by $Mn(Mo)O_3F_3$ octahedra is 12 (Figure 3b).

dx.doi.org/10.1021/jp302020f | J. Phys. Chem. C 2012, 116, 10162−10170

Table 5. Core Levels of Cs-Containing Crystals

compound	BE (Cs $3d_{5/2}$), eV	BE (O 1s), eV	BE (F 1s), eV	Δ(Cs−O), eV	Δ(Cs−F), eV	ref
Cs_3PO_4	724.1	530.3	-	−193.8	-	43
$Cs_4P_2O_7$	724.0	530.4	-	−193.6	-	43
$CsClO_4$	724.4	532.9	-	−191.5	-	43
$CsCrO_4$	723.3	529.0	-	−194.3	-	43
$Cs_2Cr_2O_7$	722.7	529.1	-	−193.6	-	44
CsB_3O_5	724.4	531.4	-	−193.0	-	45
Cs_2SO_4	724.3	531.2	-	−193.1	-	46
$CsMnMoO_3F_3$	724.5	530.6	684.3	−193.9	−40.2	this study
CsF	724.2	-	682.6	-	−41.6	43

Table 6. Core Levels of Mo-Containing Crystals

compound	BE (Mo $3d_{5/2}$), eV	BE (O 1s), eV	BE (F 1s), eV	Δ(Mo−O), eV	Δ(Cs−F), eV	ref
MoO_3	232.8	530.8	-	298.0	-	47
MoO_3	232.7	530.5	-	297.8	-	48
MoO_3	232.9	530.7	-	297.8	-	49
MoO_3	232.5	530.4	-	297.9	-	50
$CuMoO_4$	232.9	530.8	-	297.9	-	47
$Ce_2(MoO_4)_3$	232.3	529.9	-	297.6	-	48
Bi_2MoO_6	232.5	530.3	-	297.8	-	49
Na_2MoO_4	232.2	530.1	-	297.9	-	51
$CaMoO_4$	232.6	530.5	-	297.9	-	52
$MnMoO_4$	233.0	531.0	-	298.0	-	29
$CsMnMoO_3F_3$	233.0	530.6	684.3	297.6	451.3	this study

Rather low values of thermal parameters B_{iso} for all atoms (Table 2) allow us to suppose the absence of any dynamic structural disorder in $CsMnMoO_3F_3$. On the other hand, the largest B_{iso} values for Cs and F/O show that their vibrations, compared to central atoms Mn and Mo, are characterized by a pronounced anharmonicity parameter which can be determined as $\delta \approx \langle x^2 \rangle / a_0^2$, where $x = B_{iso}/8\pi^2$ is an amplitude of atom vibration, according to ref 23. Moreover, because fluorine and oxygen atoms are not localized in the cubic structure of $CsMnMoO_3F_3$, there would exist a statistical disorder of the atoms. Taking into account the structural features considered above, we have tried to find a structural transformation on cooling below room temperature. Such a transformation would be related to the positional ordering and/or displacement of F/O and Cs atoms.

Any abnormal behavior of heat capacity in cooling−heating calorimetric measurements which could be associated with the phase transitions in $CsMnMoO_3F_3$ was not found. This experimental result is not strange because, for example, elpasolite-like crystals with the same degree of anharmonic vibrations of ligands and some other atoms do not undergo the phase transitions until helium temperatures.[24] Nevertheless, it is necessary to point out that the calorimetric method used by us is not sufficiently sensitive to detect small heat effects induced by the phase transitions with the displacive mechanism or second-order transformations far from the tricritical point. In the latter case, the phase transition enthalpy (or entropy) can be rather significant, but its change takes place over a wide temperature range with a consequent small heat capacity peak at the phase transition point.

Figure 4 shows the temperature dependence of the inverse magnetic susceptibility χ^{-1} obtained in field heating at H = 10 Oe after zero-field cooling. In a wide temperature range ∼100−300 K, this parameter follows the Curie−Weiss law $\chi^{-1} \sim (T - \Theta)$ with a rather significant value of $\Theta \approx -80$ K (dashed line in Figure 4). Such behavior proves the existence of the antiferromagnetic interaction in $CsMnMoO_3F_3$. Below 100 K,

Table 7. Core Levels of Mn-Containing Crystals

compound	BE (Mn $2p_{3/2}$), eV	BE (O 1s), eV	BE (F 1s), eV	Δ(Mn−O), eV	Δ(Mn−F), eV	ref
MnO	640.9	530.0	-	−110.9	-	54
Mn_2O_3	641.2	529.8	-	−111.4	-	54
	641.9	530.2	-	−111.7	-	60
MnO_2	641.9	529.5	-	−112.4	-	54
	642.8	530.2	-	−112.6	-	29
	642.3[a]	530.2	-	−112.1	-	57
	642.2	529.7	-	−112.5	-	60
$MnPO_4$	641.9	531.8	-	−110.1	-	54
$MnSO_4 \cdot H_2O$	641.9	532.2	-	−109.7	-	54
$MnMoO_4$	641.7	531.0	-	−110.7	-	29
$LaMnO_3$	641.4	529.1[b]	-	−112.3	-	55
$LiMn_2O_4$	641.9	530.1	-	−111.8	-	56
	641.2	529.9	-	−111.3	-	61
$LiMnTiO_4$	642.8	530.2[c]	-	−112.6	-	62
$CsMnMoO_3F_3$	641.8	530.6	684.3	−111.2	42.5	this study
MnF_2	642.8	-	-	-	-	58
MnF_3	642.8	-	-	-	-	58
MnF_2	642.4	-	684.7	-	42.3	59

[a]After correction of Mn $2p_{3/2}$ peak attribution. [b]Lower BE component. [c]Main component.

dx.doi.org/10.1021/jp302020f | J. Phys. Chem. C 2012, 116, 10162−10170

there are two peculiarities in the temperature dependence of χ^{-1}. The first is a deviation from linear dependence, and the second one is connected with a strong decrease of χ^{-1} below ~20−25 K. One can suppose that these effects are associated with the appearance of some kind of magnetic ordering in the oxyfluoride under study.

It is interesting to compare the results concerning inverse magnetic susceptibility in $CsMnMoO_3F_3$ to those in the related fluorides with the *Fd*-3*m* structure.[25] Almost the same complicated temperature behavior of $\chi^{-1}(T)$ was observed in $CsMgFeF_6$, having one kind of paramagnetic ion in the structure. Recall that, according to the examination by electron paramagnetic resonance, the Mn ion in $CsMnMoO_3F_3$ was also found only in the divalent state. On the other hand, $CsMnFeF_6$ (with two kinds of paramagnetic ions) shows, at about 170 K, the deviation from the Curie−Weiss law to lower values of $\chi^{-1}(T)$ that is a characteristic for the appearance of ferrimagnetic interaction.[16]

The survey photoemission spectrum of $CsMnMoO_3F_3$ is shown in Figure 5. All spectral features detected were successfully attributed to constituent element core levels or Auger lines, except for the weak C 1s line. A comparatively narrow dominant component of the C 1s line was related to adventitious hydrocarbons adsorbed at the surface from air, and a low-intensity additive component at 288.2 eV was attributed to carbonate species. The valence band spectrum is shown in Figure 6. A mixed-states band with two components at 6.5 and 10.4 eV is found at the top of the valence band. At higher BE, a band formed by a mix of Cs 5s and O 2s states is observed. The intensive line at 28.9 eV is related to F 2s states. In Figures 7−11, the representative element core levels Mo 3d, O 1s, Mn 2p, F 1s, and Cs 3d are shown. It should be noted that a weak intensity shoulder at the low-energy side of practically all the element peaks was detected, as it seems, due to the difference charging effect.[26] The relative element ratio estimated for the powder sample is Cs:Mn:Mo:O:F = 0.11:0.06:0.07:0.21:0.55 that is in reasonable consistency with nominal composition Cs:Mn:Mo:O:F = 0.11:0.11:0.11:0.33:0.33 for Cs content, but an enrichment of the surface by fluorine is evident. The calculations were made without carbon signal accounting. The Auger parameters defined for Cs, O, and F are α_{Cs} = 1292.7, α_O = 1041.9, and α_F = 1341.2 eV. The Auger parameter of molybdenum, calculated for Mo $3d_{5/2}$ and Mo $M_{45}N_{23}V$ peaks, is α_{Mo} = 414.3 eV. The Auger parameter of manganese is α_{Mn} = 1171.0 eV as found for Mn $2p_{3/2}$ and Mn $L_{23}M_{23}M_{23}$ peaks. The Auger lines Mo $M_{45}N_{23}V$ and Mn $L_{23}M_{23}M_{23}$ are shown in Figures 1S and 2S (Supporting Information). The suite of the element core levels and Auger lines measured for $CsMnMoO_3F_3$ is shown in Table 4. Comparatively, the BE values obtained for Cs $4d_{5/2}$ and F 1s core levels in $CsMnMoO_3F_3$ are in good relation with the BE values of 76.7 and 684.9 eV earlier obtained for the core levels in another fluoromolybdate, $Cs_2MoO_2F_4$.[27] As for the Mo $3d_{5/2}$ line, the BE value obtained in $CsMnMoO_3F_3$ is similar with the value 232.5 eV reported in $Rb_2KMoO_3F_3$.[28]

It is interesting to evaluate the chemical bonding effects in $CsMnMoO_3F_3$ using constituent element core level parameters measured by XPS. When metal interacts with fluorine, oxygen, or other anion-forming elements, a redistribution of electron density occurs as a shift of valence electrons. This process results in some variations of the electronic structure of inner shells of both the cations and anions. The effect can be easily detected as a variation of the core level BE values measured by XPS, and for example, BE (Ti $2p_{3/2}$) variation is as high as ~8 eV if we compare titanium metal and Na_2TiF_6.[22,29−31] For the selected chemical class of compounds, the effect is less pronounced and can be occasionally smashed by the surface charging effect typically observed for dielectric materials. As it was shown previously, the BE difference parameter is more suitable and more sensitive for chemical bonding analysis of dielectric crystals.[32−34] Many chemical classes of crystals containing such individual anions as O^{2-}, S^{2-}, Se^{2-}, and Br^- were analyzed using the parameter, and a different character of selected cation−anion pairs has been found.[32−42] In comparison to that, $CsMnMoO_3F_3$ contains the anion complex, and respectively, specific effects can be supposed due to a competitive valence electron transfer from metals to O^{2-} and F^- ions.

It is suitable to use BE differences Δ(Cs−O) = BE (O 1s) − BE (Cs $3d_{5/2}$) and Δ(Cs−F) = BE (F 1s) −BE (Cs $3d_{5/2}$) for the characterization of Cs−O and Cs−F bonding. A shift of valence electrons from cesium to anions decreases the inner shell screening that induces an increase of BE (Cs $3d_{5/2}$) value. In parallel, the values of BE (O 1s) or BE (F 1s) decrease. Finally, lower values of Δ(Cs−O) or Δ(Cs−F) indicate higher ionicity of Cs−O or Cs−F bonds. A representative suite of Cs-containing crystals measured by XPS is shown in Table 5. The value of Δ(Cs−O) in oxides is in the range of −(193.0−194.3) eV with only one evident exception for $CsClO_4$ where the measured BE (O 1s) seems to be drastically overestimated due to the high hydrofility of the perchlorate surface.[43] The value of Δ(Cs−O) obtained for $CsMnMoO_3F_3$ is among the lowest values known for Cs-containing oxides, and that points out a very high ionicity of Cs−O bonds in this oxyfluoride. Contrary to that, the value of Δ(Cs−F) found in $CsMnMoO_3F_3$ is noticeably higher than in CsF, indicating the lower ionicity of Cs−F bonds in $CsMnMoO_3F_3$. So, the presence of fluorine increases the ionicity of Cs−O bonds, and the presence of oxygen decreases the ionicity of Cs−F bonds.

The representative collection of molybdate crystals is shown in Table 6. The BE difference Δ(Mo−O) = BE (O 1s) − BE (Mo $3d_{5/2}$) is used for the characterization of Mo−O bonding. One can see that the range of Δ(Mo−O) values in molybdates, including $MnMoO_4$, is as narrow as 297.8−298.0 eV with only one exception for $Ce_2(MoO_4)_3$ displaying 297.6 eV. Comparatively, the value as low as Δ(Mo−O) = 297.6 eV is obtained in $CsMnMoO_3F_3$ which indicates a considerably more ionic character of Mo−O bonds in this oxyfluoride in reference to that in typical molybdates. Mo−F bonding in $CsMnMoO_3F_3$ can be described by the BE difference value of Δ(Mo−F) = BE (F 1s) − BE (Mo $3d_{5/2}$) = 451.3 eV. A comparison with fluorides, however, can not be currently produced because XPS measurements of Mo-contained fluorides are not known in the literature. As to other oxyfluorides, complex Mo 3d doublets were recorded in nonstoichiometric compounds $(NH_4)_yMoO_{3-x}F_x$ ($x < 1$; $y \leq 0.3$ where a mix of Mo^{5+}/Mo^{6+} states was established by XPS and EPR).[53]

A suite of Mn-containing oxides is shown in Table 7 where BE differences Δ(Mn−O) = BE (O 1s) − BE (Mn $2p_{3/2}$) and Δ(Mn−F) = BE (F 1s) − BE (Mn $2p_{3/2}$) are applied as bonding-related parameters. It is evident that, in pure manganese oxides and $MnMoO_4$, the level of Δ(Mn−O) decreases with a manganese valence increase. The situation with Mn-containing compounds is more complicated. Commercial $MnPO_4$ and $MnSO_4 \cdot H_2O$ samples were measured in ref 54, and BE (O 1s) seems to be overestimated due to the surface

hydration. Strong surface hydration was also reported for the $LaMnO_3$ surface.[55] A mixed manganese valence should be supposed for $LiMn_2O_4$.[56,61] Strong possible deviations from stoichiometry and complex cation distribution over octahedral/tetrahedral sites were found for the $LiMnTiO_4$ spinel.[62−64] Thus, the value of Δ(Mn−O) in $CsMnMoO_3F_3$ is intermediate between that in MnO and $MnMoO_4$ molybdate and that in Mn_2O_3. This energy shift appeared to be induced by the presence of fluorine in the crystal lattice of $CsMnMoO_3F_3$. Comparatively, the value of Δ(Mn−F) in $CsMnMoO_3F_3$ is higher than that in MnF_2. So, the ionicity of Mn−F bonds in $CsMnMoO_3F_3$ is decreased by the presence of O^{2-} ions.

CONCLUSIONS

The structural, magnetic, and electronic parameters of $CsMnMoO_3F_3$ oxyfluoride are elucidated in the present study. The statistical disorder is found for Mn^{2+}/Mo^{6+} ions in octahedral positions. The anion sublattice is also completely disordered at room temperature. Interesting bonding effects are obtained for $CsMnMoO_3F_3$ oxyfluoride by XPS observation. For all cations, the ionicity of oxide bonds M−O (M = Cs, Mo, Mn) is increased in reference to that in oxides. Contrary to that, the ionicity of fluoride bonds M−F (M = Cs, Mo, Mn) is decreased in comparison to that in fluorides. So, oxyfluorides could show specific bonding features.

The results obtained in the present study make single-crystal growth of $CsMnMoO_3F_3$ and precise investigations of heat capacity, thermal expansion, structure, and magnetic properties in a wide temperature range topical. To throw light on a complicated behavior of the inverse susceptibility on temperature variation, the neutron investigations of magnetic structure are also needed.

ASSOCIATED CONTENT

Supporting Information

Crystallographic information in a CIF file. Auger line Mo $M_{45}N_{23}V$ and a complex of Auger lines of manganese and cesium in $CsMnMoO_3F_3$. This material is available free of charge via the Internet at http://pubs.acs.org.

AUTHOR INFORMATION

Corresponding Author

*Phone: +7 (383) 3308889. Fax: +7 (383) 3332771. E-mail: atuchin@thermo.isp.nsc.ru.

Notes

The authors declare no competing financial interest.

ACKNOWLEDGMENTS

We thank Dr. A.M. Ziatdinov for the electron paramagnetic resonance measurements. This study was partly supported by SB RAS (Grant 28).

REFERENCES

(1) Maggard, P. A.; Nault, T. S.; Stern, C. L.; Poeppelmeier, K. R. *J. Solid State Chem.* **2003**, *175*, 27−33.
(2) Marvel, M. R.; Lesage, J.; Baek, J.; Halasyamani, P. S.; Stern, C. L.; Poeppelmeier, K. R. *J. Am. Chem. Soc.* **2007**, *129*, 13963−13969.
(3) Chamberlain, J. M.; Albrecht, T. A.; Lesage, J.; Sauvage, F.; Stern, C. L.; Poeppelmeier, K. R. *Cryst. Growth Des.* **2010**, *10*, 4868−4873.
(4) Fry, A. M.; Seibel, H. A.; Lokuhewa, I. N.; Woodward, P. M. *J. Am. Chem. Soc.* **2012**, *134*, 2621−2625.
(5) Atuchin, V. V.; Isaenko, L. I.; Kesler, V. G.; Lin, Z. S.; Molokeev, M. S.; Yelisseyev, A. P.; Zhurkov, S. A. *J. Solid State Chem.* **2012**, *187*, 159−164.
(6) Pausewang, G.; Rüdorff, W. *Z. Anorg. Allgem. Chem.* **1969**, *364*, 69−87.
(7) Babel, D.; Pausewang, G.; Viebahn, W. *Z. Naturforsch. B* **1967**, *22*, 1219−1220.
(8) Mattes, R.; Leimkühler, V.; Nagel, A. *Z. Anorg. Allg. Chem.* **1990**, *582*, 131−142.
(9) Ravez, J.; Peraudeau, G.; Arend, H.; Abrahams, S. C.; Hagenmüller, P. *Ferroelectrics* **1980**, *26*, 767−769.
(10) Peraudeau, G.; Ravez, J.; Hagenmüller, P.; Arend, H. *Solid State Commun.* **1978**, *27*, 591−593.
(11) Flerov, I. N.; Fokina, V. D.; Bovina, A. F.; Bogdanov, E. V.; Molokeev, M. S.; Kocharova, A. G.; Pogoreltsev, E. I.; Laptash, N. M. *Phys. Solid State* **2008**, *50*, 515−524.
(12) Flerov, I. N.; Gorev, M. V.; Tressaud, A.; Laptash, N. M. *Crystallogr. Rep.* **2011**, *56*, 9−17.
(13) Zvezdin, A. K.; Pyatakov, A. P. *Phys.-Usp.* **2004**, *47*, 416−421.
(14) Scott, J. F.; Blinc, R. *J. Phys.: Condens. Matter* **2011**, *23*, 113202.
(15) Choi, S. G.; Wang, S.-J.; Park, H.-H.; Hong, M. P.; Kwon, K.-H. *J. Vac. Sci. Technol. A* **2010**, *28*, 1−5.
(16) Watanabe, N.; Nakayama, H.; Fukao, K.; Munakata, F. *J. Appl. Phys.* **2011**, *110*, 023519.
(17) Lobanov, M. V.; Abakumov, A. M.; Sidorova, A. V.; Rozova, M. G.; D'yachenko, O. G.; Antipov, E. V.; Hadermann, J.; Van Tendeloo, G. *Solid State Sci.* **2002**, *4*, 19−22.
(18) Alekseeva, A. M.; Abakumov, A. M.; Rozova, M. G.; Antipov, E. V.; Hadermann, J. *J. Solid State Chem.* **2004**, *177*, 731−738.
(19) Saratovsky, I.; Lockett, M. A.; Rees, N. H.; Hayward, M. A. *Inorg. Chem.* **2008**, *47*, 5212−5217.
(20) Udovenko, A. A.; Laptash, N. M. *Acta Cryst. B* **2008**, *64*, 305−311.
(21) Solovyov, L. A. *J. Appl. Crystallogr.* **2004**, *37*, 743−749.
(22) *Handbook of X-ray Photoelectron Spectroscopy*; Wagner, C. D., Riggs, W. M., Davis, L. E., Moulder, J. F., Muilenberg, G. E., Eds.; Perkin-Elmer Corp., Phys. Elect. Div.: Minnesota, 1979.
(23) Vaks, V. G. *Introduction to the Microscopic Theory of Ferroelectrics*; Nauka: Moscow, 1973 (in Russian).
(24) Fokina, V. D.; Flerov, I. N.; Gorev, M. V.; Molokeev, M. S.; Vasiliev, A. D.; Laptash, N. M. *Ferroelectrics* **2007**, *347*, 60−64.
(25) Paus, D.; Hoppe, R. *Z. Anorg. Allg. Chem.* **1976**, *426*, 83−94.
(26) Atuchin, V. V.; Alekseeva, O. A.; Kesler, V. G.; Pokrovsky, L. D.; Sorokina, N. I.; Voronkova, V. I. *J. Solid State Chem.* **2006**, *179*, 2349−2355.
(27) Nefedov, V. I.; Kokunov, V. V.; Buslaev, V. A.; Porai-Koshits, M. A.; Gustyakova, M. P.; Il'in, E. G. *Zh. Neorg. Khim.* **1973**, *18*, 931−934.
(28) Atuchin, V. V.; Gavrilova, T. A.; Isaenko, L. I.; Kesler, V. G.; Molokeev, M. S.; Zhurkov, S. A. *Ceram. Int.* **2012**, *38*, 2455−2459.
(29) Nefedov, V. I. *X-ray photoelectron spectroscopy of chemical compounds: Handbook*; Khimia: Moscow, 1984.
(30) Barr, T. L. *J. Vac. Sci. Technol. A* **1991**, *9*, 1793−1805.
(31) Guittet, M. J.; Crocombette, J. P.; Gautier-Soyer, M. *Phys. Rev. B* **2001**, *63*, 125117.
(32) Atuchin, V. V.; Kalabin, I. E.; Kesler, V. G.; Pervukhina, N. V. *J. Electron Spectrosc. Relat. Phenom.* **2005**, *142*, 129−134.
(33) Atuchin, V. V.; Kesler, V. G.; Pervukhina, N. V.; Zhang, Z. *J. Electron Spectrosc. Relat. Phenom.* **2006**, *152*, 18−24.
(34) Atuchin, V. V.; Kesler, V. G.; Pervukhina, N. V. *Surf. Rev. Lett.* **2008**, *15*, 391−399.
(35) Ramana, C. V.; Atuchin, V. V.; Becker, U.; Ewing, R. C.; Isaenko, L. I.; Khyzhun, O. Yu.; Merkulov, A. A.; Pokrovsky, L. D.; Sinelnichenko, A. K.; Zhurkov, S. A. *J. Phys. Chem. C* **2007**, *111*, 2702−2708.
(36) Atuchin, V. V.; Pokrovsky, L. D.; Khyzhun, O. Yu.; Sinelnichenko, A. K.; Ramana, C. V. *J. Appl. Phys.* **2008**, *104*, 033518.
(37) Atuchin, V. V.; Galashov, E. N.; Khyzhun, O. Yu.; Kozhukhov, A. S.; Pokrovsky, L. D.; Shlegel, V. N. *Cryst. Growth Des.* **2011**, *11*, 2479−2484.

(38) Atuchin, V. V.; Zhang, Z. *J. Nucl. Mater.* **2012**, *420*, 222−225.
(39) Atuchin, V. V.; Kesler, V. G.; Parasyuk, O. V. *Surf. Rev. Lett.* **2007**, *14*, 403−409.
(40) Atuchin, V. V.; Golyashov, V. A.; Kokh, K. A.; Korolkov, I. V.; Kozhukhov, A. S.; Kruchinin, V. N.; Makarenko, S. V.; Pokrovsky, L. D.; Prosvirin, I. P.; Romanyuk, K. N.; Tereshchenko, O. E. *Cryst. Growth Des.* **2011**, *11*, 5507−5514.
(41) Atuchin, V. V.; Isaenko, L. I.; Kesler, V. G.; Tarasova, A. Yu. *J. Cryst. Growth* **2011**, *318*, 1000−1004.
(42) Tarasova, A. Yu.; Isaenko, L. I.; Kesler, V. G.; Pashkov, V. M.; Yelisseyev, A. P.; Denysyuk, N. M.; Khyzhun, O. Yu. *J. Phys. Chem. Solids* **2012**, *73*, 674−682.
(43) Morgan, W. E.; Van Waser, J. R.; Stec, W. J. *J. Am. Chem. Soc.* **1973**, *95*, 751−755.
(44) Allen, G. C.; Curtis, M. T.; Hooper, A. J.; Tucker, P. M. *J. Chem. Soc., Dalton Trans.* **1973**, *1973*, 1675−1683.
(45) Atuchin, V. V.; Pokrovsky, L. D.; Kesler, V. G.; Maklakova, N. Yu.; Yoshimura, M.; Ushiyama, N.; Matsui, T.; Kamimura, K.; Mori, Y.; Sasaki, T. *Opt. Mater.* **2003**, *23*, 377−383.
(46) Wahlqvist, M.; Shchukarev, A. *J. Electron Spectrosc. Relat. Phenom.* **2007**, *156−158*, 310−314.
(47) Haber, J.; Machej, T.; Ungier, L.; Ziółkowski, J. *J. Solid State Chem.* **1978**, *25*, 207−218.
(48) Barr, T. L.; Fries, C. G.; Cariati, F.; Bart, J. C. J.; Giordano, N. *J. Chem. Soc., Dalton Trans.* **1983**, *1983*, 1825−1829.
(49) Uchida, K.; Ayame, A. *Surf. Sci.* **1996**, *357−358*, 170−175.
(50) Ramana, C. V.; Atuchin, V. V.; Kesler, V. G.; Kochubey, V. A.; Pokrovsky, L. D.; Shutthanandan, V.; Becker, U.; Ewing, R. C. *Appl. Surf. Sci.* **2007**, *253*, 5368−5374.
(51) Ho, S. F.; Contarini, S.; Rabalais, J. W. *Chem. Phys. Lett.* **1987**, *133*, 171−175.
(52) Im, H.-N.; Choi, M.-B.; Jeon, S.-Y.; Song, S.-J. *Ceram. Int.* **2011**, *37*, 49−53.
(53) Laptash, N. M.; Nikolenko, Y. M.; Mishchenko, N. M. *Z. Neorg. Khim.* **1997**, *42*, 765−768.
(54) Nelson, A. J.; Reynolds, J. G.; Roos, J. W. *J. Vac. Sci. Technol. A* **2000**, *18*, 1072−1076.
(55) Stephan, K.; Hackenberger, M.; Kießling, D.; Richter, F.; Wendt, G. *Chem. Eng. Technol.* **2002**, *25*, 559−564.
(56) Ramana, C. V.; Massot, M.; Julien, C. M. *Surf. Interface Anal.* **2005**, *37*, 412−416.
(57) Sui, N.; Duan, Y.; Jiao, X.; Chen, D. *J. Phys. Chem. C* **2009**, *113*, 8560−8565.
(58) Carver, J. C.; Schweitzer, G. K.; Carlson, T. A. *J. Chem. Phys.* **1972**, *57*, 973−982.
(59) Li, X.; Lu, J.; Peng, G.; Jin, L.; Wei, S. *J. Phys. Chem. Solids* **2009**, *70*, 609−615.
(60) Fetisov, A. V.; Kozhina, G. A.; Fetisov, V. B.; Pastukhov, E. A. *J. Appl. Spectrosc.* **2011**, *78*, 240−244.
(61) Manoharan, S. S.; Singh, B. *Synth. React. Inorg., Met.-Org., Nano-Met. Chem.* **2008**, *38*, 148−151.
(62) Arillo, M. A.; López, M. L.; Pico, C.; Veiga, M. L.; Jiménez-López, A.; Rodríguez-Castellón, E. *J. Alloys Compd.* **2001**, *317−318*, 160−163.
(63) Yoo, K. S.; Cho, N. W.; Oh, Y.-J. *Solid State Ionics* **1998**, *113−115*, 43−49.
(64) Arillo, M. A.; Guello, G.; López, M. L.; Martin, P.; Pico, C.; Veiga, M. L. *Solid State Sci.* **2005**, *7*, 25−32.